

Structural, electronic and optical properties of HgS under pressure using FP-LAPW method

P. K. Saini^{1,2*}, D.S. Ahlawat¹, D.Singh³

¹Department of Physics, Chaudhary Devi Lal University, Sirsa (India)125055

²Department of Physics, Govt PG College, Hansi (India) 125033

³ Department of Physics, MM University, Ambala (India)

-----***-----

Abstract: - We report a detailed investigation on structural, electronic and optical properties of mercury chalcogenide HgS in zinc blende (ZB) and high pressure rocksalt (RS) structures using DFT based FP-LAPW (WIEN2k) method. Apart from ground state and structural properties, the work is also reported on band structure, Fermi energy, band gap, mechanical properties and optical properties including dielectric functions, refractive index, loss function etc. Furthermore, the calculated results have been compared with the earlier available experimental and theoretical results.

Keywords: Band gap, Elastic constants, FP-LAPW, DFT and Optical properties

I. Introduction

The mercury chalcogenides, HgX (X= S, Se, Te) have enormous technological importance in optoelectronic applications such as emitter, tunable lasers, photoconductor, IR detector, electrostatic imaging, photoelectric conversion devices [1-7]. The phase transition of HgS from cinnabar structure under ambient conditions, to rocksalt structure under high pressures has been studied in theories and experiments [8-13]. A. Fleszar et. al. reported that the unusual properties of mercury chalcogenides are due to the interaction between the localized semicore d electron with the valence p electron [14]. Only a few results have been reported for HgX compounds, when compared with other II-VI compounds and their alloys [15-18]. Cardona et. al. [19] has reported the electronic band structure and the phonon dispersion relations of the mercury chalcogenides in ZB structure. The band gap is a very important parameter which affects the electrical, magnetic and optical properties of semiconducting materials. The band gaps of most III-V and II-VI compounds have been correctly measured [20-21]. On the basis of published data, most of the studies were carried out experimentally and there was smaller effort to understand the theoretical electronic structure and optical properties particularly at high pressure which is an important mode for better understanding for this class of materials. The present work deals with the detailed study about the structural, electronic, mechanical and optical properties of HgS in ZB and high pressure RS phases by using the first-principle calculations based on density functional theory (DFT) within generalized gradient approximation. The structure of this paper is as follows: in Section II we discuss the procedures employed for the *ab initio* calculations. Section III and IV presents some important results obtained for structural and electronic properties of HgS. The calculated optical properties have been presented in Section V. Finally, section VI contains the summary of obtained results and conclusion.

II. Methodology

The calculations have been performed using the FP-LAPW method [22-24] within the framework of DFT [25] as implemented in the WIEN2K [26] code. For structural properties, the exchange-correlation potential was calculated using the generalized gradient approximation (GGA). It has been observed that the GGA method underestimates the magnitude of the energy band gap below the experimental value, while the energy band gap value computed by EV-GGA method is very near to its experimental value. So in addition to that for the calculation of electronic properties only the Engel-Vosko (EV) scheme was applied [27]. The alternative basis sets (APW+lo) are used inside the atomic spheres for important *l*-orbitals (partial waves). For the total energy convergence, the basis functions in the IR were expanded up to $R_{mt} K_{max} = 7.0$. The maximum value of *l* were taken as $l_{max} = 10$, while the charge density is Fourier expanded up to $G_{max} = 12$. For the calculation of electronic properties we have used 72 k-points in the irreducible Brillouin zone for structural optimization. Moreover, a semi-relativistic approximation (no spin orbit effects included) was employed, whereas the core levels were treated fully relativistic. Further the optical properties are obtained from frequency dependent dielectric function for which the imaginary part of dielectric tensor can be computed from the electronic band structure of HgX. For the calculation of linear optical properties we have used 3000 k-points. In the present study for all three compounds, 5p, 5d, 6s orbitals of Hg, 3s, 3p, 3d orbitals of S, 4s, 4p, 4d of Se and 5s, 5p, 5d of Te have been treated as valence states.

III. Structural Properties

Equilibrium volume and equilibrium lattice constants are calculated at both the ZB and high pressure RS phases for which the total energies are computed here by changing the cell volume. The calculated total energies are fitted according to Murnaghan equation of state (EOS) [28] to obtain the equilibrium lattice constant, bulk modulus and the other elastic constants etc. The Total energy versus volume data for the ZB (B3) and RS (B1) phases of HgS are shown in the Figure 1(a) and 1(b).

The optimized lattice constants of HgS is obtained as 5.99 Å in zinc blende phase whereas it is found 5.57 Å for RS phase under the application of high pressure at about 16.1 GPa, respectively. At this high pressure HgS is found to be existing in RS phase in more stable form. The calculated structural parameters of HgS have been listed in Table 1, along with some previous theoretical and experimental measurements.

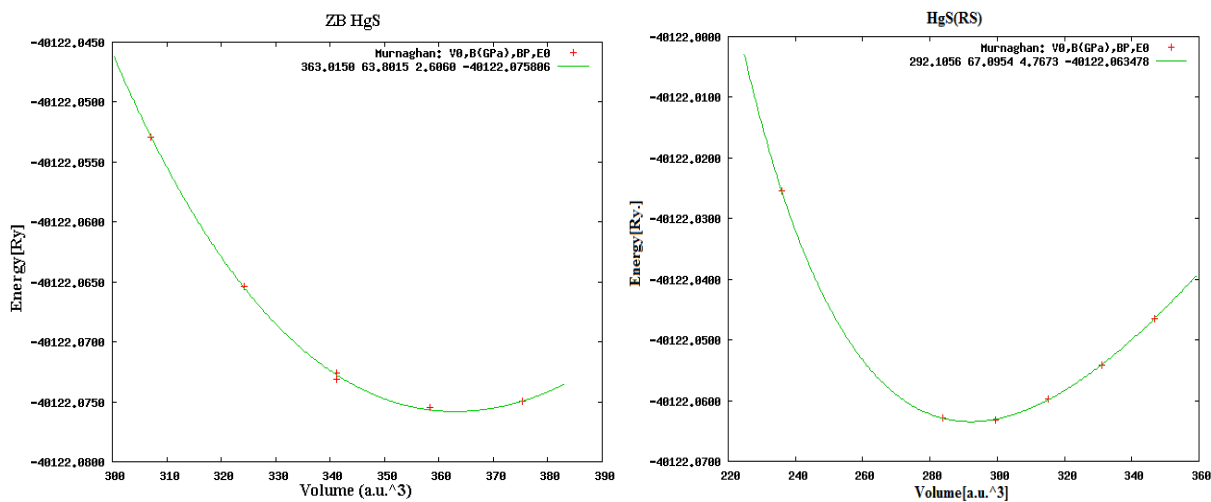


Figure 1(a): Volume vs Total energy of HgS in ZB phase. Figure 1(b): Volume vs Total energy of HgS in RS phase.

It shows that our calculated value for lattice constant overestimates more than 2.3%, whereas results for bulk modulus are nicely agreed with their experimental values. It can be clearly seen that the GGA calculated lattice constants overestimate the experimental values, which is a general trend that GGA usually overestimates this parameters. It can also be seen that the lattice constant of HgS found to be reduced at high pressure whereas bulk modulus and derivation of bulk modulus (B_0) are found to be increased with the increase in pressure.

Table 1: Calculated equilibrium lattice constants (a_0), bulk modulus B_0 , and the pressure derivative of bulk modulus (B'_0) along with the related experimental data, and the other theoretical works for HgS, in ZB and RS phases.

HgS	Calculations	a_0 (Å)	B_0 (GPa)	B'_0
ZB phase	Present work	5.99	63.80	2.60
	Theory [Ref.29]	5.97	-	-
	Exp. [Ref.30]	5.85	68.6	-
RS phase	Present work	5.57	67.09	4.76

Further, the elastic constants have also been calculated for the ZB of HgS and presented in the Table 2. To obtain the elastic constants of zinc blende structure, we have used a numerical first- principles calculation by computing the components of the stress tensor for small strains, using the method developed by Charpin and integrated in WIEN2k code [26]. There are three independent elastic constants namely C_{11} , C_{12} , and C_{44} for a cubic crystal. The mechanical stability of cubic crystal should match with the conditions: $C_{11}-C_{12}>0$, $C_{44}>0$, $C_{11}+2C_{12}>0$. The calculated elastic constants are found to obey the cubic stability conditions including the fact that C_{12} must be smaller than C_{11} . Further, other elastic constants like shear modulus G, Young modulus E, anisotropic parameter A, Kleinmann parameter ξ and Poisson ratio γ have also been

calculated using the important relations [31] for the ZB phase of HgS and presented in the Table 2. To the best of our knowledge, there is no experimental data available for comparison of the calculated elastic properties of ambient ZB phase. However, our calculated result may be very useful for further experimental and theoretical study of HgS material.

Table 2. The calculated elastic constants C_{ij} (GPa), bulk modulus B (GPa), shear modulus G , Young modulus E , anisotropic parameter A , Kleinmann parameter ξ and Poisson ratio γ for HgS in the ZB phase.

HgS	Calculations	C_{11}	C_{12}	C_{44}	B	G	E	A	ξ	γ
ZB phase	Present work	70.47	46.52	43.30	54.50	30.35	76.79	0.88	0.75	0.26
	Others	-	-	-	-	-	-	-	-	-

IV. Electronic Properties

Band Structure

The band structures for both the phases of HgS have been shown in Figure 2(a) and 2(b). In both cases they are obtained by the FP-LAPW (WIEN2k) method within EV-GGA for improving the accuracy in the band gap. The approach (EV) provides a better band splitting. The overall band structure profiles for both the phases are found to be similar. However, a little difference in the band position on energy scale may be seen as in the case of ambient phase, the lowest lying band in the valence band region are found at -12.2 eV. It mainly arises from the 3s states of S while the bands just below E_F , that is, the top of the valence bands are composed of Hg-d and S-p states. The d states of Hg are more prominent in the valence bands than the s states. The bottom of the conduction bands is composed of the hybridization states of Hg-s and S-p, and also some states from Hg-d. Similarly, a little difference may be seen on the energy scale in the electronic band structure of RS phase of HgS calculated by FP-LAPW method. Furthermore, one can see from the Figure 2(b), in high pressure rock salt phase of HgS that the hybridization interaction of the d electrons with anion p electrons leads to a repulsion of the involved states. An increased width of the upper valence bands and a decrease in the band gap has been observed. This may occur because of S- 3p states are pushed up in energy towards the Hg-6s derived conduction bands by p-d interaction. Thus, comparing LAPW-GGA and LAPW-EV-GGA calculations in the zincblende and rocksalt phases, one can see that the band structures are very similar, except the band gap at Γ point for the GGA result which is smaller than EV-GGA result.

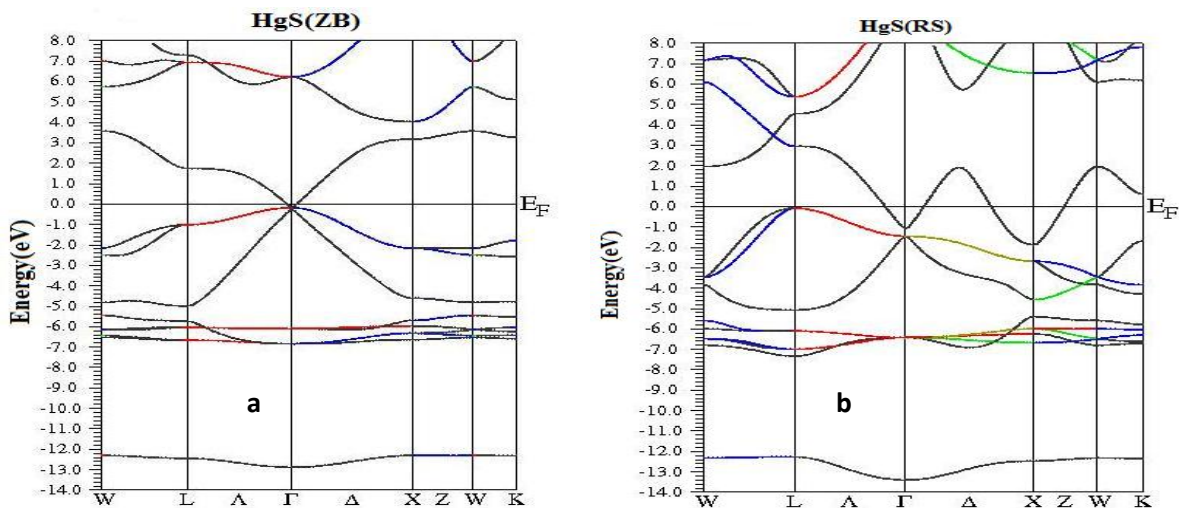


Figure 2(a-b): Band structure of HgS in ZB and RS Phases using EV-GGA.

Band Gap

The energy band gap is the difference between the top of the valence band and the bottom of conduction band as shown in the Figure 2(a-b) for both the phases of HgS. We calculated the band gap for ZB phase using LDA and GGA schemes and the calculated values of the energy gap are given in the Table 3 along with the earlier reported theoretical work [29,34] and experimental values [32,33]. One can notice from the calculated results of band gap that both LDA and GGA underestimate the energy gaps as comparatively to their experimental values. However, GGA yields slightly larger

energy gaps than LDA. Further, we have used EV-GGA scheme to improve the band gap [26]. The band gap is calculated by use of EV-GGA and their values are found to be improved and lying closer to the experimental results [33]. Similarly, it is calculated that band gap for high pressure RS phase is obtained to be reduced as a function of pressure as one can see from the comparative study of band structures and partial DOS for both ZB and RS phases. This may be due to the fact as mentioned above in high pressure rock salt (B1) phase of HgS that the hybridization interaction of the d electrons with anion p electrons leads to a repulsion of the involved states which is responsible for an increased width of the upper valence bands region and hence have decrease in the band gap. It can be noticed for the rocksalt phase, the conduction band and the valence band overlap at several places. On the basis of this, it can be explained that the rocksalt phase of HgS under high pressure has metallic properties [12].

Table 3 : The calculated direct-band gap for zinc blende phase of HgS along with the other theoretical and experimental work.

Material	Calculations	Direct band gap(eV) at Γ point
HgS	Present work (using EV-GGA)	-0.1
	Present work (using GGA)	-0.16
	Present work (using LDA)	-0.56
	Theory(Ref. [29])	-0.6
	Theory(Ref. [34])	0.28
	Experimental(Ref. [32])	-0.5
	Experimental(Ref. [33])	-0.1

The calculated band structures of HgS indicate a negative direct band gap equal to -0.1eV. Thus the obtained data is indicating to have an overall good agreement with the experimental results collected from the literature.

V. Optical Properties

Under this section the optical properties of HgS have been considered. The core states are treated fully relativistically while the valence and semi-core states are treated semirelativistically (*i.e.* ignoring the spin-orbit coupling). The dispersion of the real and imaginary parts of dielectric function, $\epsilon_1(\omega)$ and $\epsilon_2(\omega)$, for ZB HgS are shown in the Figure 3 and 4, respectively. The observed spectra $\epsilon_2(\omega)$ shows the threshold energy occurring at 0.12 eV. There are three major energy spectral peaks situated at 3.01 , 6.05 (principal peak), and 7.29 eV.

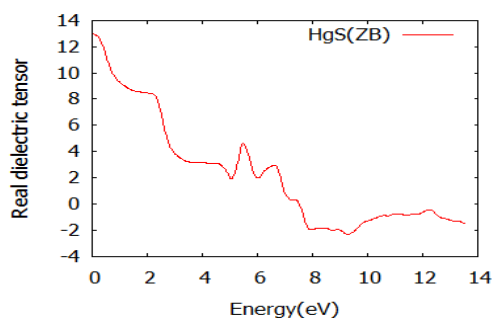


Fig.3: Real dielectric function of $\epsilon^1(\omega)$ HgS(ZB).

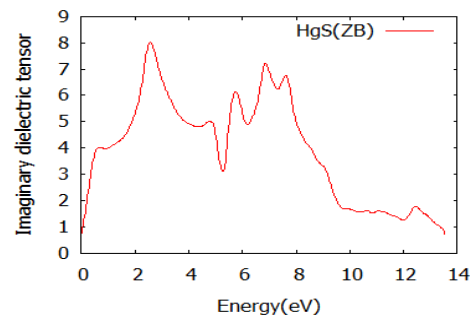


Fig.4: Imaginary dielectric function $\epsilon^2(\omega)$ of HgS(ZB).

The highest peak in $\epsilon_2(\omega)$ at about 3.01 eV is 8.01, corresponds to the transition from occupied Hg-s to unoccupied S-s band states. From the analysis of Figure 3, the calculated static dielectric constant $\epsilon_1(0)$ without any contribution from lattice vibration is equal to about 12.9 presented in the Table 4. The wide band energy gap yields a smaller value of $\epsilon_1(0)$. First main and highest peak value 8.3 of $\epsilon_1(\omega)$ exists at energy 2.4 eV , second peak value 4.8 exists at energy 5.7 eV and third peak value 2.82 exists at energy 6.72 eV while all other peaks have negative value -1.90, -1.41, and -1.43 at energies 10.10, 11.52, and 12.83 eV, respectively. The calculated static dielectric constants $\epsilon_1(0)$ is compared with the experimental values presented in the Table 4. It is noticed that a smaller energy gap yields a larger $\epsilon_1(0)$ value. It could be explained on the basis of the Penn model [35]. Further, the Figure 5 and 6 shows the calculated real $\epsilon_1(\omega)$ and imaginary dielectric function $\epsilon_2(\omega)$ for the HgS compound in RS phase. It is noted that the $\epsilon_2(\omega)$ shows a large peak (located at 3.2 eV) for HgS in RS phase. The calculated static dielectric constant $\epsilon_1(0)$ for RS HgS without any contribution from lattice vibration is

equal to about 17.6 presented in Table 4. There is no experimental data available for static dielectric constant in ZB and RS phases in the literature, so comparison is not possible in this case.

The Figure 7 represents the refractive index spectra for the HgS compound in ZB phase. This shows that the refractive index is significant only upto of 2.42 for HgS beyond this energy it drops sharply. The theoretically calculated static refractive index 3.6 for HgS given in the Table 5. The Figure 8 represents the refractive index spectra for the HgS compound in RS phase. This shows that the refractive index is significant only upto 2.7 for HgS and beyond this energy it drops sharply. The theoretically calculated static refractive index is 4.3 for HgS (RS) phase which is given in the Table 5. There is no experimental data available for refractive index of ZB and RS phase in the literature, so comparison is not possible in this case.

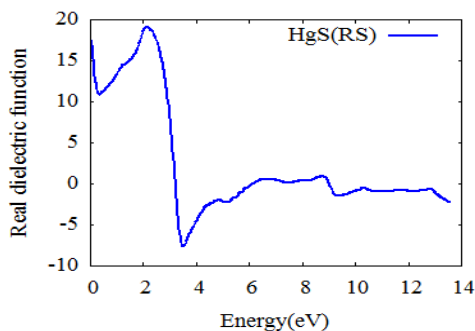


Fig. 5: Real dielectric function $\epsilon_1(\omega)$ of HgS(RS).

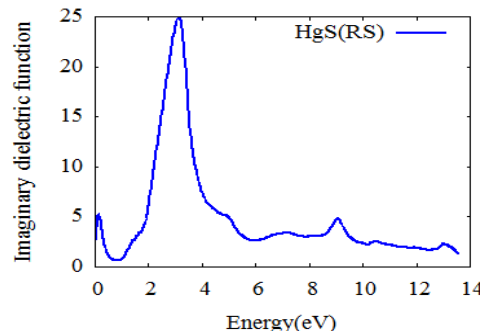


Fig. 6: Imaginary dielectric function $\epsilon_2(\omega)$ of HgS(RS).

Table 4: Calculated value of static dielectric constant for cubic ZB and RS phases of HgS.

Compound	Phase	Calculation	Static dielectric constant, $\epsilon_1(0)$
HgS	ZB	Present work	12.9
		Others	-
	RS	Present work	17.6
		Others	-

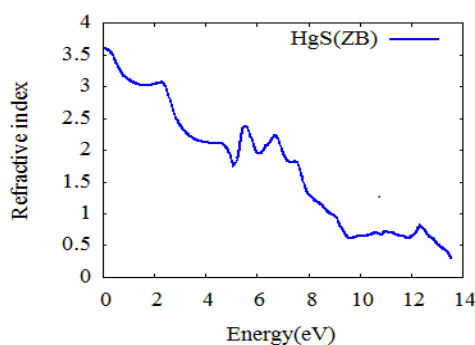


Fig.7: Refractive index of HgS(ZB).

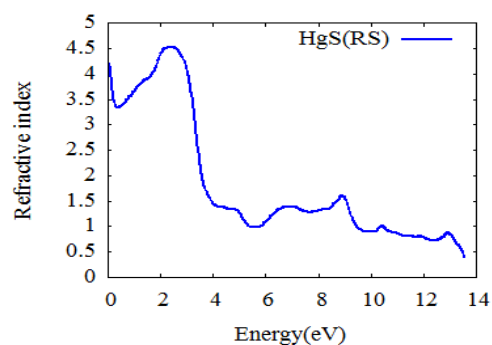


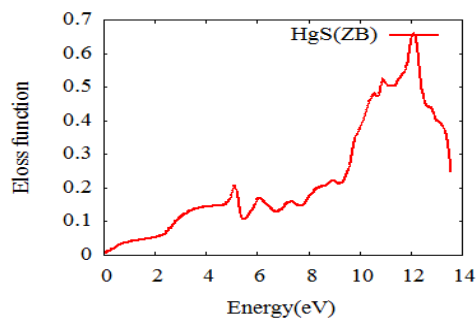
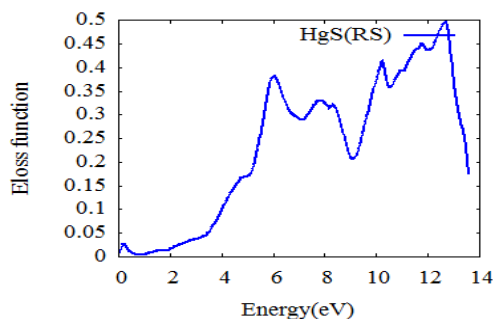
Fig.8: Refractive index of HgS(RS).

The EELS is a valuable tool for investigating various aspects of the material under investigation. The positions of the single electron excitation peaks are related to the joint density of states between the conduction and valence bands. The electrons, which excite the atoms and electrons of the outer shell is called valence loss or valence interband transitions. In the case of interband transitions, which consist mostly of plasmon excitations, the scattering probability for volume losses is directly related to the energy loss function. In Figure 9, the major peak in the energy loss spectrum is connected with the plasmon peak and located at 12.22 eV for HgS in the ZB phase and the corresponding frequency is called plasma frequency (ω_p) [36].

Table 5: Calculated static refractive index for cubic ZB and RS phases of HgS.

HgS	Calculations	Refractive index
ZB Phase	Present work	3.6
	Others	-
RS Phase	Present work	4.3
	Others	-

Further, the Figure 10 represents the most prominent peak in the energy loss spectrum associated with the plasmon peak and located at 12.88 eV for HgS in the RS phase. To the best of our knowledge, we are not aware about the data available for comparison of the calculated results of HgS for the optical dispersions. These properties may be helpful for future predictions about the above said compound in ZB and RS phase.


Fig. 9: Eloss function of HgS(ZB).

Fig. 10: Eloss function of HgS(RS).

VI. Conclusions

In this paper we studied the structural, electronic and optical properties of HgS materials using the first principles calculations. The obtained results for band structures and DOS show that this compound have inverted band structure and showing semi-metallic behaviour at ZB phase. The calculated band structures of HgS indicate a negative direct band gap equal to -0.1eV. Thus the obtained data is indicating to have an overall good agreement with the experimental results collected from the literature. The metallic character increases under high pressure RS phase due to crossing of conduction band at Fermi level in different high symmetric directions in band structures. All the peak structures in the imaginary part of the dielectric function $\epsilon_2(\omega)$ are shifted towards lower energies with increase in peaks height in RS phases of HgS. We have also found that the theoretically obtained values of static dielectric constants $\epsilon_1(0)$ and static refractive index increases with decreasing energy gap which are in well agreement with the Penn model. The same trend has been found in the case of RS phase of HgS. Further, We have also calculated the other optical properties like dielectric function, refractive index, and eloss function spectra for ZB and RS phases of HgS compound seeking for more detail comparison with the earlier reported experimental results. The calculation details presented could be useful for further experimental investigations and we hope that can be used to cover the lack of data for this compound.

References:

- [1] N. Tokyo, J. Appl. Phys. **46**(1975) 4857.
- [2] C. R. Whisett, J. G. Broerman, C.J. Summers, in: R.K. Willardson, A. C. Beer (Eds.), Semiconductors and Semimetals, Vol.16, Academic Press, New York, **Ch-4** (1981).
- [3] P. P. Hankare, V.M. Bhuse, K.M. Garadkar, A.D. Jadhav, Mater. Chem. Phys. **71** (2001) 9982.
- [4] V. Vankatasamy, N. Jayaraju, S.M. Cox, C. Thambidurai, M. Mathe and J. L. Stickney, J. Electroanal. Chem. **195** (2006) 589.
- [5] S. Y. Girgis, A. M. Salem, M. S. Selim, J. Phys: Condens. Matter **19** (2007)116213.

- [6] K.A. Higginson, M. Kuno, J. Bonevich, S.B. Qadri, M. Yousuf, H. Mattoussi, J. Phys. Chem. B **106**(2002) 39.
- [7] H. Wang, J.J. Zhu, Ultrason. Sonochem. **11**(2004) 293.
- [8] T. Huang and A. L. Ruoff, J. Appl. Phys. **54** (1983)5459.
- [9] T. L. Huang and A.L. Ruoff, Phys. Rev. B **31**(1985) 5976.
- [10] A. Werner, H. D. Hochheimer, K. Strossner, and A. Jayaraman, Phys. Rev. B **28** (1983)3330.
- [11] M. A. Blanco, J. M. Recio, A. Costales, and R. Pandey, Phys. Rev. B **62** (2000) R10 599.
- [12] M. Catti, Phys. Rev. Lett. **87** (2001)035504.
- [13] M. Catti, Phys. Rev. B **65** (2002)224115.
- [14] A. Fleszar and W. Hanke , Phys. Rev. B **71**(2005) 045207
- [15] S. R. Sun and Y.H. Dong, Phys. Rev. B **72**(2005)174101, Phys. Rev. B **73**(2006)113201.
- [16] F. Boutaiba, A. Zaoui and M. Ferhat , Superlattice Microstruct. **46** (2009) 823.
- [17] V. Kumar , A. K. Shrivastava and V. Jha , J. Phys. Chem. Solids **71** (2010)1513.
- [18] A. S.Verma , R.K.Singh and S.K. Rathi , Physica B **404**(2009) 4051.
- [19] M. Cardona, R. K.Kremer , R. Lauck , G. Siegle , A. Muñoz and A. H. Romero, Phys. Rev. B **80** (2009)195204
- [20] C. Y. Moon and S.H. Wei, Phys. Rev. B **74**(2006)045205.
- [21] O. Madelung (ed) 2003 Semiconductors: Data Handbook 3rd edn (Berlin: Springer)
- [22] D. D. Koelling and B. N. Harmon , J. Phys. C: Solid State Phys. **10** (1977) 3107
- [23] K. Schwarz, P. Blaha and G.K.H. Madsen , Comput. Phys. Commun. **147**(2002) 71
- [24] G.K.H. Madsen,P. Blaha , K. Schwarz, E. Sjöstedt and L. Nordström , Phys. Rev. B **64** (2001)195134
- [25] P. Hohenberg and W. Kohn, Phys. Rev. **136**(1964) 864; W. Kohn and L.J. Sham, Phys. Rev. **140** (1965)A1133
- [26] P. Blaha , K. Schwarz , G.K.H. Madsen , D. Kvasnicka and J. Luitz 2001 WIEN2k, An Augmented Plane Wave + Local Orbitals Program for Calculating Crystal Properties (Wein: Karlheinz Schwarz, Techn. University)
- [27] E. Engel, S.H. Vosko, Phys. Rev. **47** (1993) 13164.
- [28] F. D. Murnaghan, Proc. Natl. Acad. Sci. USA,**30** (1944) 244.
- [29] X. Chen, A. Mintz, J. Hu, X. Hua, J. Zinck, J. Vac. Sci. Technol. B **13** (1995) 4.
- [30] O. Madelung (Ed.), Landolt Börnstein: Numerical Data and functional Relationships in Science and Technology, Springer, Berlin, Vol. **17b** (1982).
- [31] P.K. Saini, D. Singh and D. S. Ahlawat, Chalcogenide Letters, **11**, No. 9(2014) 405.
- [32] W. H. Strehlow, E.L. Cook, J. Phys. Chem. **2** (1973) 163.
- [33] K. Dybko, W. Szuszkiewicz, E. Dynowska, W. Paszkowicz, B. Witkowska, Physica B **256** (1998) 629.
- [34] A. Fleszar, W. Hanke, Phys. Rev. B **71**(2005) 045207.
- [35] D. R. Penn, Phys. Rev. **128**(1962)2093.
- [36] P. Nozieres, Phys.Rev. Lett. **8** (1959)1.